Inorganica Chimica Acta 507 (2020) 119548

Contents lists available at ScienceDirect

Inorganica Chimica Acta

journal homepage: www.elsevier.com/locate/ica

Research paper

Binuclear manganese-iron complexes containing ferrocenyl thiosemicarbazones: Biological activity and carbon monoxide-releasing properties

Madelyn L. Lawrence, Steven M. Shell, Floyd A. Beckford*

Department of Natural Sciences, The University of Virginia's College at Wise, 1 College Avenue, Wise, VA 24293, United States

1. Introduction

Carbon monoxide (CO) is well known for its toxicity in large doses. CO has a high affinity for both myoglobin and hemoglobin and will bind to the heme group of both of these proteins. This binding will reduce the amount of oxygen available to the organism which can ultimately lead to symptoms such as fatigue and headaches [1]. Because of its toxicity, CO was once thought to have no function in living organisms, but upon detailed study, it was found that CO is produced within humans as a byproduct of heme breakdown by heme oxygenase (HO) [2]. Heme oxygenase exists in the forms HO-2, HO-3, and HO-1. The HO-1 form, an inducible form, is very important when it comes to injury and stress. In the absence of HO-1, the concentrations of CO are much lower than normal, and this can result in important enzymes not being up-regulated. The negative side effects to this include blood clotting, slow healing, and poor resistance to infection [3].

Another important characteristic of carbon monoxide is that it can exhibit proapoptotic effects in some dysregulated hyperproliferative cells such as cancer cells [4]. Carbon monoxide has been shown to be useful as an anti-inflammatory, anti-microbial, and cytoprotective agent [5]. Once it was observed that CO could perform these important functions, scientists went in search of molecules that contained CO, the release of which would produce these effects. These searches led to the development of carbon monoxide-releasing molecules (CORMs) [6–9]. The research done in this field has shown that metal carbonyls have great potential to be CO-releasing molecules. Ruthenium and manganese are among the metals that have the ability to serve multiple biological functions [10–12], which makes them prime templates for CORMs. These CORMs can release the gas differently and/or react differently depending on several factors; one factor is irradiation by light of different wavelengths. Complexes that are susceptible to photoemission of CO are generally referred to as photoCORMs. However, there are other mechanisms for CO emission from compounds [6,13–15].

Thiosemicarbazone (TSC) ligands have been extensively researched [16] and have shown a large range of chemotherapeutic activity: cytotoxic [17], anti-malaria [18], antifungal [19], and DNA-cleaving activity [20]. The ligands, when linked to metal ions, can enhance and broaden the activity of the overall resulting complex [21]. Therefore, ligation to an active CORM unit could enhance the chemotherapeutic properties of both moieties.

The medicinal application of ferrocene and its derivatives is an active field of research [22]. Ferrocene in particular has been regularly investigated because it a neutral, chemically stable and nontoxic molecule [23]. Some ferrocenyl compounds are highly active against several diseases, including cancer, malaria and bacterial infections [24–30]. Of special note, is the fact that the ferrocene unit has been shown to broaden the activity spectrum of tamoxifen, a breast cancer drug [31]. Breast cancer tumors can be classified as ER(+) and ER(−) types. The ER(+) tumors are susceptible to hormone therapy by selective estrogen receptor modules (SERMs) while the ER(−) tumors are not. Consequently, tamoxifen, is only effective on the ER(+) tumors, particularly the ERα subtype, and it is not effective on hormone-independent tumors. The ferrocifens, tamoxifen molecules incorporating a ferrocene unit, were the first molecules shown to be active against both hormone-dependent and hormone-independent breast cancer cells [31]. In light of the above discussion, attaching the ferrocene unit to another metal center, such as in CORMs, could potentially broaden the medicinal potential of the final compounds.

This research aimed to pair a ferrocenyl TSC ligand with a {Mn$(CO)_3$} subunit to create a photoactive complex. In general, the ferrocene TSC ligands were structurally varied in two ways with respect to the alkyl group R^1 in Fig. 1. The first was based on the use of acetylferrocene, where R^1 is a methyl group. The second variation is when ferrocene carboxaldehyde, where the R^1 is a hydrogen, was used in the synthesis of the ligands. The ligand was also varied by changing the R^2 group attached to the amine nitrogen (NH) in Fig. 1. This R^2 group was either a hydrogen, a methyl group, or a phenyl group. Consequently, a set of six complexes were synthesized, characterized, and tested for their biological activities as well as their propensity to act as photoCORMs.

* Corresponding author.
E-mail address: fab5b@uvawise.edu (F.A. Beckford).

https://doi.org/10.1016/j.ica.2020.119548
Received 28 October 2019; Received in revised form 12 February 2020; Accepted 21 February 2020
Available online 25 February 2020
0020-1693/

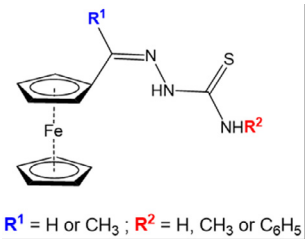

Fig. 1. Proposed structure of the synthesized ligands.

2. Experimental

2.1. Material and methods

Elemental analyses were performed by Galbraith Laboratories, (Knoxville, TN, USA). ^{1}H NMR spectra were obtained using a Bruker Avance III 400 MHz spectrometer. UV/Vis spectra were measured using a Perkin Elmer Lambda 25 UV/Vis spectrophotometer. IR spectra were recorded on a Perkin Elmer Spectrum 100 FT-IR spectrophotometer. ESI-MS mass spectra were recorded on an Advion expression-L CMS. Cyclic voltammetric data was collected on a Bioanalytical Systems Inc. Epsilon potentiostat on a C3 cell stand at 296 K. A platinum disc working electrode, a Pt-wire counter electrode, and an Ag/AgCl reference electrode were used and all solutions were deoxygenated with nitrogen before measurement. The photochemical experiments were carried out using an Aldrich® Micro Photochemical Reactor (ALDKIT001) with a blue (435–445 nm spectral range) LED light ring and a purple LED light ring (ALDRP2, 400–410 nm). The UV illumination was carried out using a 3UV-38 (UVP, LLC) lamp. Absorbance measurements for the antimicrobial and anticancer assays were carried out using a BioTek Cytation 1 microplate reader. Figures were created with Perkin Elmer's ChemDraw. All reagents and solvents were purchased from commercial sources.

2.2. Synthesis and characterization

The ligands **L1**-**L6** were synthesized (Scheme 1) by slightly modifying the procedures reported [32,33] for **L4**-**L6**. In short, to an aqueous suspension of the thiosemicarbazide (40 cm^3) was added an equivalent amount of the acetylferrocene or ferrocene carboxaldehyde as a solution in ethanol (30 cm^3). A few drops of glacial acetic acid were added and the red reaction mixture heated at reflux for 2 h without the exclusion of air during which a red–orange suspension formed. After cooling to room temperature, the reaction mixture was filtered and the resulting solid dried at the vacuum line. (The reaction may be run in straight ethanol as well.)

The general synthesis of the manganese complexes from the thiosemicarbazone ligands is illustrated by Scheme 2. In the synthesis, the solid thiosemicarbazone ligand was added under argon flow into a flame dried Schlenk flask. Dried acetone (30 cm^3) was added to the flask and the mixture degassed for 5 min. The manganese pentacarbonyl bromide complex was quickly mixed in with the ligand at a 1.1:1 mol ratio and the reaction mixture degassed for another 5 min. The solution flask was kept covered with aluminum foil, and the reaction mixture was refluxed for 3 h. After the reaction time, the solvent was removed by rotary evaporation. Methylene chloride was used to redissolve the solid; filtration through Celite was done before pentane was added for recrystallization. The products were collected via vacuum filtration. The CORM complexes were labelled as **C1**-**C6** and can be seen in Scheme 2. **C1**-**C3** are based on TSCs from ferrocene carboxaldehyde while **C4**-**C6** are the acetylferrocene-based complexes. **C1** and **C4** have a common hydrogen, **C2** and **C5** have a methyl group, and **C3** and **C6** have a phenyl group on the amine nitrogen.

2.3. Solution stability tests

All six CORM complexes were tested for their solution stability when exposed to ambient light versus being kept in the dark. Each of the six complexes was dissolved to derive 3 mL of 10 μM solution. Two solutions were made for each of the six complexes. One solution was kept in the ambient light while the other was kept in the dark. A UV–Vis spectrum was taken of each solution at 0, 24, 48 and 72 h. The spectra were then compared to obtain information on the stability of each complex.

2.4. Photoreactivity tests

Photoreactivity of the complexes was investigated by timed illuminations of the dissolved complexes under different wavelengths of light. UV (365 nm), blue (435 nm), and purple (410 nm) light were used. The UV light (365 nm) was most effective, so testing was continued with only UV light. The time of illumination differed from 15 s intervals to 30 min intervals and in-between. For each complex, 150 μL of a 2 mM stock solution, in acetonitrile, of each complex was diluted to

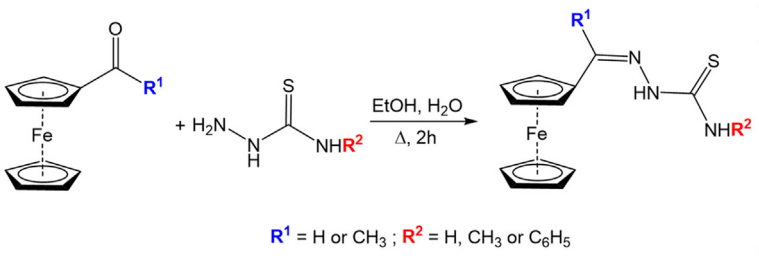

Ligand	R^1	R^2
L1	H	H
L2	H	CH_3
L3	H	C_6H_5
L4	CH_3	H
L5	CH_3	CH_3
L6	CH_3	C_6H_5

Scheme 1. Our synthesis of the ligands **L1**: Yield: 94%, dark orange powder. Elemental analysis for $C_{12}H_{13}FeN_3S$ Calc.: C 50.19, H 4.56, N 14.63. Found: C 50.61, H 3.91, N 14.32. ^{1}H NMR (400 MHz, dmso-d$_6$): δ 11.14 (s, 1H), 7.99 (s, 1H), 7.89 (s, 1H), 7.88 (s, 1H), 7.57(s, 1H), 4.72 (d, 2H), 4.40 (d, 2H), 4.20 (s, 5H). IR (cm^{-1}): 3428, 3375, 3116, 1599, 1527, 1285, 811. **L2**: Yield: 89%, dark orange powder. Elemental analysis for $C_{13}H_{15}FeN_3S$ Calc.: C 51.84, H 5.02, N 13.95. Found: C 52.13, H 4.40, N 13.61. ^{1}H NMR (400 MHz, dmso-d$_6$): δ 11.17 (s, 1H), 8.13 (s, 1H), 7.89 (s, 1H), 4.72 (d, 2H), 4.42 (d, 2H), 4.20 (s, 5H), 2.99 (s, 3H). IR (cm^{-1}): 3345, 3297, 3131, 1611, 1548, 1302, 811. **L3**: Yield: 97%, orange-red powder. Elemental analysis for $C_{18}H_{17}FeN_3S$ Calc.: C 59.51, H 4.72, N 11.56. Found: C 59.71, H 4.20, N 11.15. ^{1}H NMR (400 MHz, dmso-d$_6$): δ 11.56 (s, 1H), 9.75 (s, 1H), 8.01 (s, 1H), 7.62 (s, 2H), 7.35 (s, 2H), 7.18 (s, 1H), 4.83 (s, 2H), 4.45 (s, 2H), 4.23 (s, 5H). IR (cm^{-1}): 3345, 3309, 3115, 1611, 1530, 1271, 817. **L4**: Yield: 68%, orange-red powder. Elemental analysis for $C_{13}H_{15}FeN_3S$ Calc.: C 51.84, H 5.02, N 13.95. Found: C 52.10, H 4.64, N 13.79. ^{1}H NMR (400 MHz, dmso-d$_6$): δ 9.93 (s, 1H), 8.07 (s, 1H), 7.64 (s, 1H), 4.79 (m, 2H), 4.37 (m, 2H), 4.17 (s, 5H), 2.17 (s, 3H). IR (cm^{-1}): 3402, 3217, 3138, 1587, 1286, 817. **L5**: Yield: 85%, orange powder. Elemental analysis for $C_{14}H_{17}FeN_3S$ Calc.: C 53.34, H 5.44, N 13.33. Found: C 53.45, H 4.78, N 13.05. ^{1}H NMR (400 MHz, dmso-d$_6$): δ 9.92 (s, 1H), 8.19 (s, 1H), 4.81 (m, 2H), 4.37 (m, 2H), 4.17 (s, 5H), 3.01 (s, 3H), 2.19 (s, 3H). IR (cm^{-1}): 3358, 3221, 1532, 1291, 815. **L6**: Yield: 89%, orange powder. Elemental analysis for $C_{19}H_{19}FeN_3S$ Calc.: C 60.49, H 5.08, N 11.14. Found: C 60.49, H 4.53, N 10.96. ^{1}H NMR (400 MHz, dmso-d$_6$): δ 10.33 (s, 1H), 9.79 (s, 1H), 7.61 (m, 2H), 7.33 (m, 2H), 7.18 (m, 1H), 4.88 (m, 2H), 4.40 (m, 2H), 4.21 (s, 5H), 2.28 (s, 3H). IR (cm^{-1}): 3339, 3272, 3095, 1589, 1514, 1262, 818.

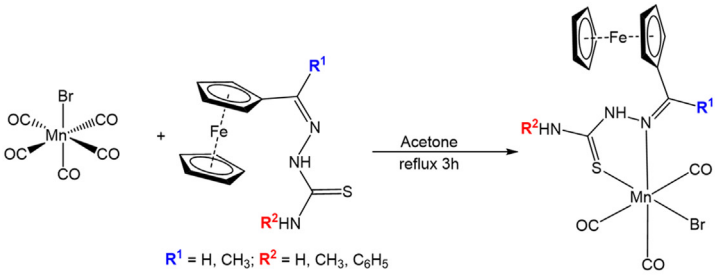

Compound	R^1	R^2
C1	H	H
C2	H	CH_3
C3	H	C_6H_5
C4	CH_3	H
C5	CH_3	CH_3
C6	CH_3	C_6H_5

Scheme 2. Synthesis and proposed structure of the manganese complexes **C1**·0.10CH_2Cl_2 Yield: 73%, orange powder. Elemental analysis for $C_{15.1}H_{13.2}BrCl_{0.2}FeMnN_3O_3S$ Calc.: C, 35.25; H, 2.59; N, 8.17. Found: C, 35.26; H, 2.36; N, 7.96. ^{1}H NMR (400 MHz, acetone-d_6): δ 10.63 (s, 1H), 8.40 (s, 1H), 8.30 (s, 2H), 4.99 (s, 2H), 4.73 (s, 2H), 4.45 (s, 5H). IR (cm^{-1}): 3462, 3250, 2020, 1903, 1607, 1532, 1255, 822. UV/Vis (CH_3CN): 317 nm. ESI-MS: *m/z* calc. for [M-3CO-Br + CH_3CN]$^+$ 383.0 Found: 382.9 **C2**·0.25CH_2Cl_2 Yield: 55%, orange powder. Elemental analysis for $C_{16.25}H_{15.5}BrCl_{0.5}FeMnN_3O_3S$ Calc.: C, 36.06; H, 2.89; N, 7.76. Found: C, 36.10; H, 2.49; N, 7.68. ^{1}H NMR (400 MHz, acetone-d_6): δ 10.40 (s, 1H), 8.62 (s, 1H), 8.30 (s, 1H), 4.91 (s, 2H), 4.71 (s, 2H), 4.42 (s, 5H), 3.22 (s, 3H). IR (cm^{-1}): 3201, 3120, 2020, 1900, 1574, 1517, 1252, 826. UV/Vis (CH_3CN): 319 nm. ESI-MS: *m/z* calc. for [M-3CO-Br + CH_3CN]$^+$ 397.0 Found: 396.9 **C3**·0.5CH_2Cl_2. Yield: 83%, deep red power. Elemental analysis for $C_{21.5}H_{18}BrClFeMnN_3O_3S$ Calc.: C, 41.34; H, 2.90; N, 6.73. Found: C, 41.28; H, 3.03; N, 6.77. ^{1}H NMR (400 MHz, acetone-d_6): δ 10.51 (s, 1H), 8.61 (s, 1H), 8.47 (s, 1H), 7.65 (s, 2H), 7.55 (s, 2H), 7.41 (s, 1H), 4.88 (s, 2H), 4.73 (s, 2H), 4.42 (s, 5H). IR (cm^{-1}): 3248, 3198, 2019, 1928, 1601, 1564, 1514,1254, 822. UV/Vis (CH_3CN): 328 nm. ESI-MS: *m/z* calc. for [M-3CO-Br + CH_3CN]$^+$ 459.0 Found: 458.9 **C4** Yield: 67%, light red–orange powder. Elemental analysis for $C_{16}H_{15}BrFeMnN_3O_3S$. Calc.: C, 36.95; H, 2.91; N, 8.08 Found: C, 37.60; H, 2.95; N, 7.87. ^{1}H NMR (400 MHz, acetone-d_6): δ 10.81 (s, 1H), 8.37 (s, 1H), 8.14 (s, 1H), 4.74 (s, 2H), 4.39 (s, 2H), 4.19 (s, 5H), 2.45 (s, 3H). IR (cm^{-1}): 3250, 3129(b), 2017, 1901, 1609, 1532, 1286, 824. UV/Vis (CH_3CN): 307 nm. ESI-MS: [M-3CO-Br]$^+$ calc.: *m/z* = 356.0, obs.: 355.8; [M-3CO-Br + CH_3CN]$^+$ calc.: *m/z* = 397.0 Found: 396.8 **C5**·0.25CH_2Cl_2. Yield: 57%, orange powder. Elemental analysis for $C_{17.25}H_{17.5}BrCl_{0.5}FeMnN_3O_3S$. Calc.: C, 37.31; H, 3.18; N, 7.57. Found: C, 37.07; H, 3.10; N, 7.64. ^{1}H NMR (400 MHz, dmso-d_6): δ 9.96 (s, 1H), 8.22 (s, 1H), 4.82 (s, 2H), 4.37 (s, 2H), 4.18 (s, 5H), 3.01 (s, 3H), 2.19 (s, 1H). IR (cm^{-1}): 3179, 2020, 1902, 1580, 1526, 1282, 824. UV/Vis (CH_3CN): 306 nm. ESI-MS: [M-3CO-Br]$^+$ calc.: *m/z* = 370.0, obs.: 369.8; [M-3CO-Br + CH_3CN]$^+$ calc.: *m/z* = 411.0 obs.: 410.9 **C6**·CH_2Cl_2. Yield: 51%, dark red power. Elemental analysis for $C_{23}H_{21}BrCl_2FeMnN_3O_3S$. Calc.: C, 40.56; H, 3.11; N, 6.17. Found: C, 40.32; H, 3.27; N, 6.72 ^{1}H NMR (400 MHz, dmso-d_6): δ 10.36 (s, 1H), 9.81 (s, 1H), 7.69 (m, 2H), 7.36 (m, 2H), 7.29 (m, 1H), 4.89 (m, 2H), 4.32 (m, 2H), 4.21(s, 5H), 2.29 (s, 3H). IR (cm^{-1}): 3366, 3184, 2019, 1930, 1599, 1565, 1364, 825. UV/Vis (CH_3CN): 313 nm. ESI-MS: [M-3CO-Br]$^+$ calc.: *m/z* = 432.0, obs.: 431.8; [M-3CO-Br + CH_3CN]$^+$ calc.: *m/z* = 473.0 obs.: 472.9.

3 mL with acetonitrile for a final concentration of 100 μM. The UV–VIS spectra were obtained after each illumination period until minimal change in the spectra was observed. IR spectroscopy was used to confirm the disappearance of CO bands after final illumination.

2.5. Antibacterial tests

The antimicrobial activity of the complexes was measured against four different strains of bacteria as reported earlier [34]. The four strains were *Enterococcus faecalis* and *Streptococcus pyogenes* which are gram-positive microbes, and *Pseudomonas aeruginosa* and *Klebsiella pneumoniae* which are gram-negative. Blue colored wells indicated no bacteria growth, purple indicated some inhibition of bacteria growth, and pink wells indicated the growth of bacteria.

2.6. Human cell cytotoxicity tests

The cytotoxicity profiles of the complexes were determined using the HEK293T cell line as we reported before [34]. Briefly, cells cultured in 1x DMEM supplemented with 10% FBS were incubated under standard growth conditions at 37 °C and 5% CO_2. The cells were harvested by trypsinization and seeded at a density of 20,000 cells/cm^3 into 96-well tissue-culture treated microtiter plates. Compound solutions or DMSO (mock-treatment) were added at a 1:100 dilution into each well, and the cultures were incubated under standard growth conditions for up to 24, 48 or 80 h post addition. Cell viability was monitored via the MTT assay. Lethal dose 50 (LD_{50}) values were estimated graphically. Assays were performed in triplicate.

3. Results and discussion

3.1. Synthesis and characterization

The thiosemicarbazone ligands used in this study were synthesized from ferrocene carboxaldehyde or acetylferrocene. The metal complexes were synthesized by reacting these ligands with manganese pentacarbonyl bromide in dry acetone at reflux temperatures. The products were recrystallized from a dichloromethane solution by precipitation with pentane. Spectroscopic and elemental analysis data confirmed the authenticity of the compounds as formulated in Schemes 1 and 2. The NMR spectra for **L1**-**L3** (Fig. S1) show the presence of the azomethine proton at 11.14, 11.17 and 11.56 ppm respectively. In the complexes corresponding to these ligands, that is **C1**-**C3**, this peak is shifted upfield by 0.5 – 1 ppm. In these complexes, the signal for the original carbonyl proton is 0.45 ppm downfield of where it was in the ligands. Similar shifts to lower fields are observed for the amine proton (s) and those of the ferrocenyl group. The solution behavior of the complexes bearing the thiosemicarbazones from acetyl ferrocene (**C4**-**C6**) is different than that described above. For instance, in these cases the azomethine proton is at lower fields relative to the free ligands. On the other hand, it does not appear that the ferrocene signals change on ligation. So, it can be suggested that the electronic communication between the CORM unit and the ligand is affected by whether we have the ketone or aldehyde kernel in the thiosemicarbazone.

The mass spectra of the complexes support the molecular formulation (Fig. S2). The major peak corresponds to the acetonitrile adduct following loss of the carbon monoxide and bromide ligands; that is [M-3CO-Br + CH_3CN]$^+$. For **C4**-**C6** the [M-3CO-Br]$^+$ is also observed at generally equal intensity. This ion is also present in **C1**, **C2** and **C3** but it is quite low intensity.

The infrared spectra of the complexes are very similar (Fig. 2). In the carbonyl region, each complex display two strong peaks near 2020 and 1900 cm^{-1}. This is characteristic of the presence of a *fac*-{Mn$(CO)_3$} unit in the complexes. The phenyl-substituted complexes have the lower-energy band at 1930 cm^{-1}. The amine peaks characteristic of the ligand moiety (3000 – 3400 cm^{-1}) show some change with both peak shifts and reduction in the number of peaks being apparent. The rest of the spectrum do show the characteristic shifts in the C═N (azomethine) and C═S (or C–S) region on ligation. (Fig. S3)

Fig. 3 shows the electronic absorption spectra for the complexes in the presence and absence of ambient light over time. For the "dark" spectra, the samples were wrapped in aluminum foil and kept in a desk drawer until just before measurement while the "light" spectra were for samples that were kept on the laboratory bench exposed to ambient

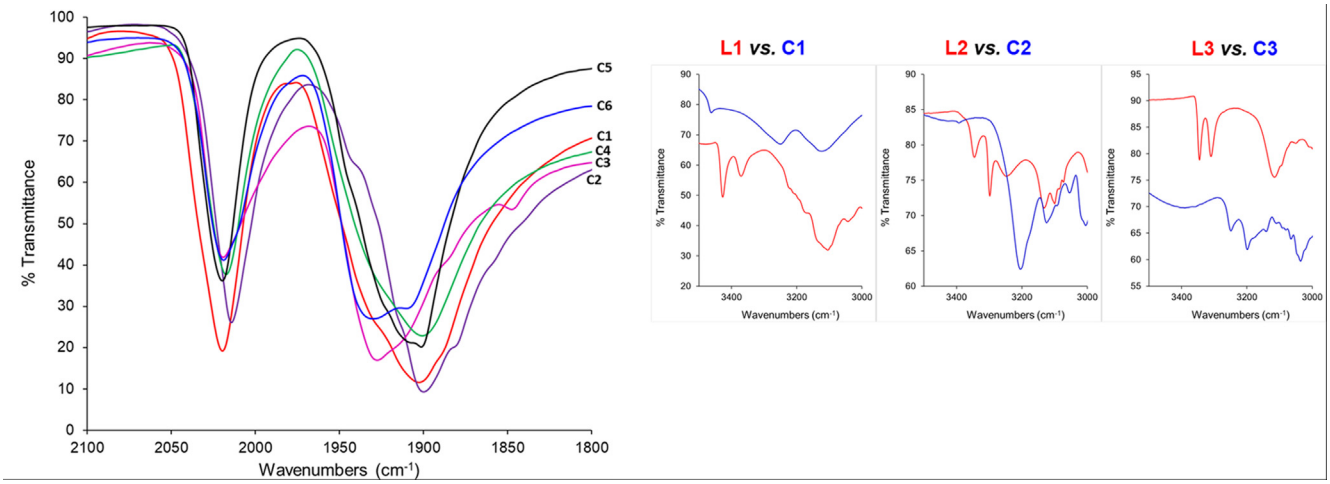

Fig. 2. Infrared spectra of the complexes in the carbonyl region. (*Inset*: Ligand comparison in the NH-region for complexes **C1**-**C3**.)

light. As can be seen from the figure, the original spectral features change slowly over the course of 24 h (and not much up to 72 h; data not shown). For the solutions exposed to ambient light, there are hypsochromic shifts for complexes **C1**-**C3** (data not shown for **C2** and **C3**) of the wavelength of maximum absorbance by as much as 13 nm. This was accompanied by moderate hyperchromic changes as well. There are no significant changes (other than small decreases in absorbance) for the solutions of these complexes that were protected from ambient light. The stability behavior of complexes **C4**-**C6** is very different. Solutions of these complexes are unaffected by exposure to ambient light with respect to changes in the main spectral features. There seemed to be some noticeable changes in the far-UV region for all the compounds but generally speaking, the complexes were stable over 24 h (and possibly up to 72 h) in the presence and absence of ambient light.

The electrochemical behavior of the compounds was investigated by cyclic voltammetry on a platinum disc electrode in the potential range 0 V to 1.0 V vs. Ag/AgCl. Voltammograms of the compounds are given in Fig. 4. The ligands show a single reversible redox couple that can logically be assigned to the ferrocene unit that is contained in it. The potentials for this couple were clustered near 0.59 V for the ligands derived from ferrocene carboxaldehyde; this is slightly higher than the average (0.57 V) for the acetylferrocene-derived analogs (Table 1).

In the complexes, the ferrocene potential shows a generalized shift to more negative values by as much as 22 mV for **C2**. In this respect, there appears to be no significant effect of the group (H or $-CH_3$) on the original carbonyl carbon. The shifts in this potential suggest that there is some electronic communication between the iron center and the manganese ion in the CORM unit. The variation of the shift is also consistent with the substituent pattern on the amine nitrogen. The complexes with the methyl substituent have the lowest potentials. This is likely due to the electron donating characteristics of alkyl groups which make the iron center easier to oxidize once it is coordinated. The electron withdrawing effect of the phenyl group reverses this effect somewhat and those complexes have more positive redox potentials. We attribute the redox couple near 0.80 V for all the complexes, to the Mn^{+}/Mn^{2+} redox couple. These are quasi-reversible peaks. It has been reported that in complexes containing a ferrocene-cyclomanganated CORM complex, the $Mn(CO)_4$ moiety was electrochemically silent up 0.60 V (vs. Fc^{+}/Fc) [35]. Other reports indicate that the manganese center in the $Mn(CO)_3$ unit of CORMs can be irreversibly oxidized at higher potentials [36]. As seen in panel **D** of Fig. 4, the complexes bearing the ferrocene carboxaldehyde-based ligands (**C1**-**C3**) show a second redox couple (E^1) at lower positive potentials. We attribute this to a manganese-based or CORM-based redox event as it is not present in the ligands and it would be suggesting that these complexes might be ligated differently by the thiosemicarbazone ligands when compared to **C4**-**C6**.

3.2. Photoreactivity investigations

We have studied the potential for the complexes to emit carbon monoxide under the influence of different wavelengths of radiation: 365 nm (UV), 405 nm (purple) and 435 nm (blue). While the ideal wavelength for photo-activation is in the range 620–850 nm [37–39], the use of higher energy radiation can potentially be used for treatment

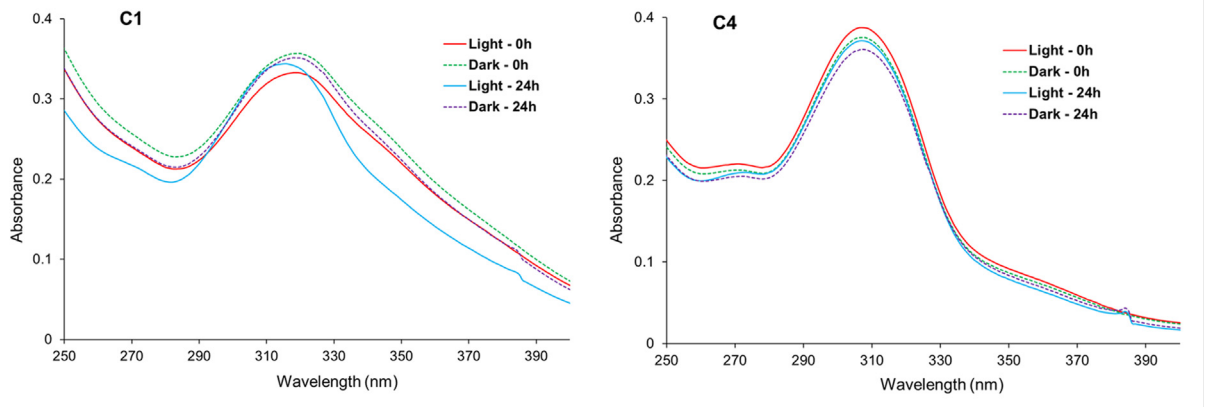

Fig. 3. Electronic absorption spectra of complexes **C1** and **C4** as a function of time and light exposure.

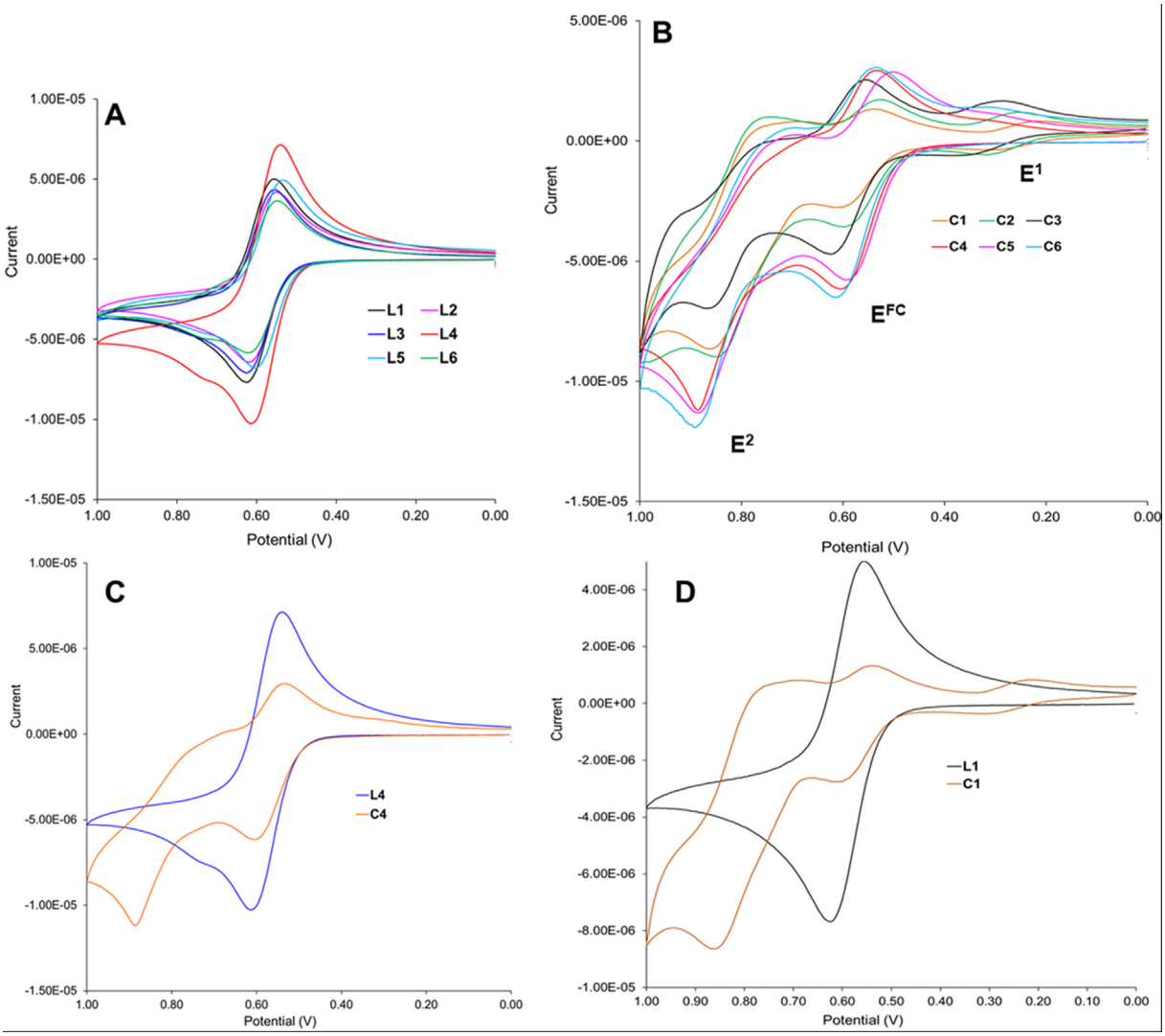

Fig. 4. Cyclic voltammograms of the compounds including comparisons between ligand and complexes.

Table 1
Potentials of the ligands and of the complexes and the changes that occur.

Compound	E^{FC}	E^{1}	E^{2}	ΔE^{FC}
L1	0.590			
L2	0.585			
L3	0.590			
L4	0.578			
L5	0.567			
L6	0.581			
C1	0.579	0.258	0.773	−0.011
C2	0.563	0.288	0.798	−0.022
C3	0.590	0.328	0.803	0
C4	0.570		0.818	−0.008
C5	0.548		0.785	−0.019
C6	0.574		0.792	−0.015

of near-surface conditions. Metal carbonyl compounds are generally photoactive [40]. At the same time, complexes containing the carbonyl ligand are uniquely amenable to infrared analysis. The rate at which CO is released from a photoCORM will depend on the solvent used as well as the electronic characteristics of the metal center. The latter point in turn will be affected by the type of ligands in the coordination sphere together with the carbonyl ligands. Our previous investigation involving a NS donor set of a thiosemicarbazone ligand [34], have shown that the CO emission rate was mainly a function of the energy of the radiation used to cause the emission. Fig. 5 show the temporal evolution of the UV–Vis spectra of the complexes before and following illumination with light. As is shown, there are noticeable changes in the spectra of the complexes upon illumination. Within the first two minutes, there is a major hypsochromic shift (of close to 13 nm) of the wavelength of maximum absorption. Over twenty minutes the spectra exhibited hyperchromic and slight bathochromic shifts. There is not much change after 20 min but the results shown for **C1** are not typical for the complexes. Closer examination of the data for **C2**-**C6** obtained using UV illumination indicate that there are two distinct phases of reaction that are characteristic of the compound. That is, each complex shows a different spectral change but in a two-part sequence. The wavelength of maximum absorption typically shows an increase in absorbance that may or may not be accompanied by a wavelength shift. This increase seems to stop around the six-minute mark; it is followed by a decrease in absorbance which plateaus around 20 min. We interpret these results as confirmation that all the complexes can be induced to liberate CO with the application of all three wavelengths of light studied.

The infrared spectra, at least for **C1**-**C3**, supports this assertion. Fig. 6 shows the initial and final infrared spectra of two complexes, **C3** and **C6**, after irradiation with 365 nm light. We observed in preliminary experiments that the blue and purple light were only minimally effective at inducing changes in the infrared spectra of the complexes. As can

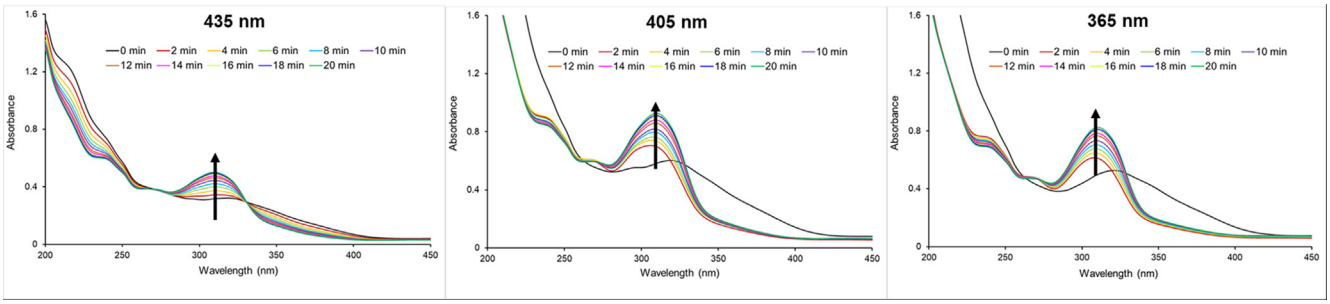

Fig. 5. Changes in the electronic absorption spectra of complexes **C1** on irradiation with different wavelengths of light.

be seen, there is a decrease in the intensity of the infrared bands attributed to the presence of the carbon monoxide ligands after 3 h of irradiation. There is hardly any change for the **C4**-**C6** complexes. So, unlike our previous report [34], it appears that these ferrocenyl thiosemicarbazone ligands are inefficient at promoting CO emission at a functional rate.

3.3. Biological activity

3.3.1. Antibacterial tests

The antimicrobial activity of the compounds was investigated using the resazurin micro-dilution assay. Four species of bacteria of different Gram stains were used studied: *Enterococcus faecalis* and *Streptococcus pyogenes* which are gram-positive microbes, and *Pseudomonas aeruginosa* and *Klebsiella pneumoniae* which are gram-negative. All four strains can have important effects on human health. *Enterococcus faecalis*, is hardly troublesome when present in normal amounts in the gut, but is a frequent cause of many serious human infections, and these may be life threatening. Infections with *E. faecalis* can be especially troublesome to treat because of their frequent resistance to multiple antibiotics. It is responsible for a large percentage of hospital-acquired infections. *Streptococcus pyogenes* is an important human pathogen that can cause a wide variety of acute infections leading to both noninvasive and invasive disease. The most common infection is streptococcal pharyngitis (so called “strep-throat”) but it can also be the cause of severe life-threatening infections including pneumonia, scarlet fever and rheumatic fever. *Pseudomonas aeruginosa* has become an important cause of gram-negative infections. Serious *Pseudomonas* infections can occur, especially in patients with weakened immune systems such as those recovering from surgery. Pseudomonal infections are complicated and can be life-threatening with blood infections and pneumonia for example, being quite possible. A significant percentage (near 13%) of the hospital-related infections are multidrug-resistant, raising the concern even higher [41]. *Klebsiella pneumoniae* are bacteria that occur commonly in the intestines. So, while normally harmless, these bacteria can cause severe infections in people with compromised immune systems. Pneumonia, bloodstream infections, wound or surgical site infections are some of the potential problems and unfortunately some *Klebsiella* bacteria have become highly resistant to antibiotics [42,43].

Fig. 7 show the physical results of the effect of the complexes on the growth of *E. faecalis*. The numerical results from the assays are given in Table 2. The information for *S. pyogenes* is not shown as the test plates for this microbe was all purple throughout. This might indicate that the bacterium is generally sensitive to the compounds but in a non-specific manner. The wells for the controls also showed a change from blue to purple (Fig. S4).

For the other bacteria, generally speaking all the complexes show good activity with estimated minimum inhibitory concentrations (MICs) typically no higher than 50 μM but on average closer to 12.5 μM. There were no significant differences in activity amongst the ligands against the various bacteria; all the ligands seem to adversely affect each bacterium in the same way. For instance, the MIC for all the ligands against *E. faecalis* was 50 μM. *P. aeruginosa* appear to be the most sensitive species to the ligands. In addition, all the bacteria were more sensitive to the complexes than to the ligands (with the exception of *P. aeruginosa*). As with the ligands though, there were no differences amongst the complexes when considering a single strain. So, it does appear that the CORM subunit has an effect on the antimicrobial properties of the complexes.

3.3.2. Acute human cell cytotoxicity

Given the effectiveness of the complexes against various bacteria, we next tested these compounds for acute cytotoxicity in human cell culture. HEK293T cells were grown in medium supplemented with increasing concentrations of compounds **C1**-**C6**. An MTT metabolism assay was then performed at 24, 48, and 80 h post-inoculation to determine the relative number of viable cells in each culture. Fig. 8 shows the percent change in cell viability relative to mock-treated cells. All six

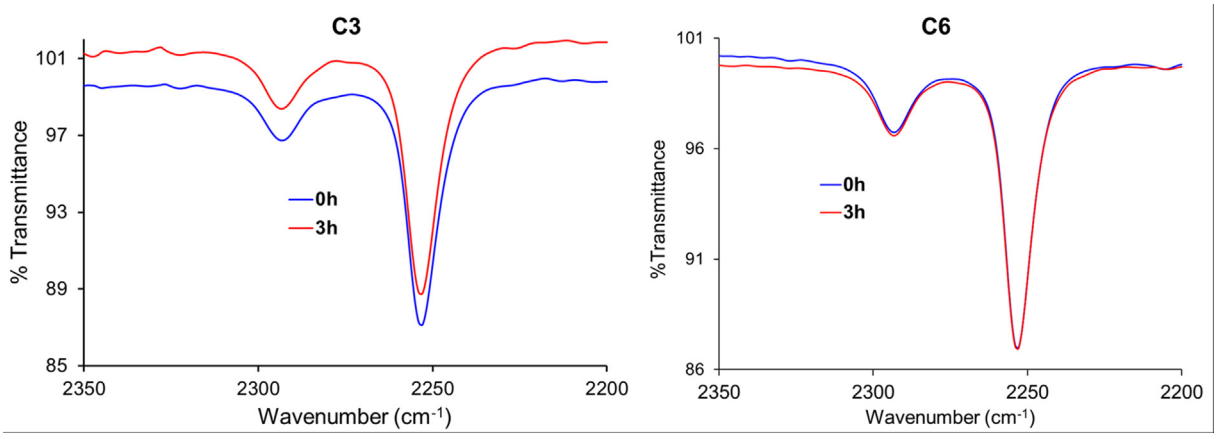

Fig. 6. Changes in the infrared spectrum of complexes **C3** and **C6** before and after irradiation with UV light.

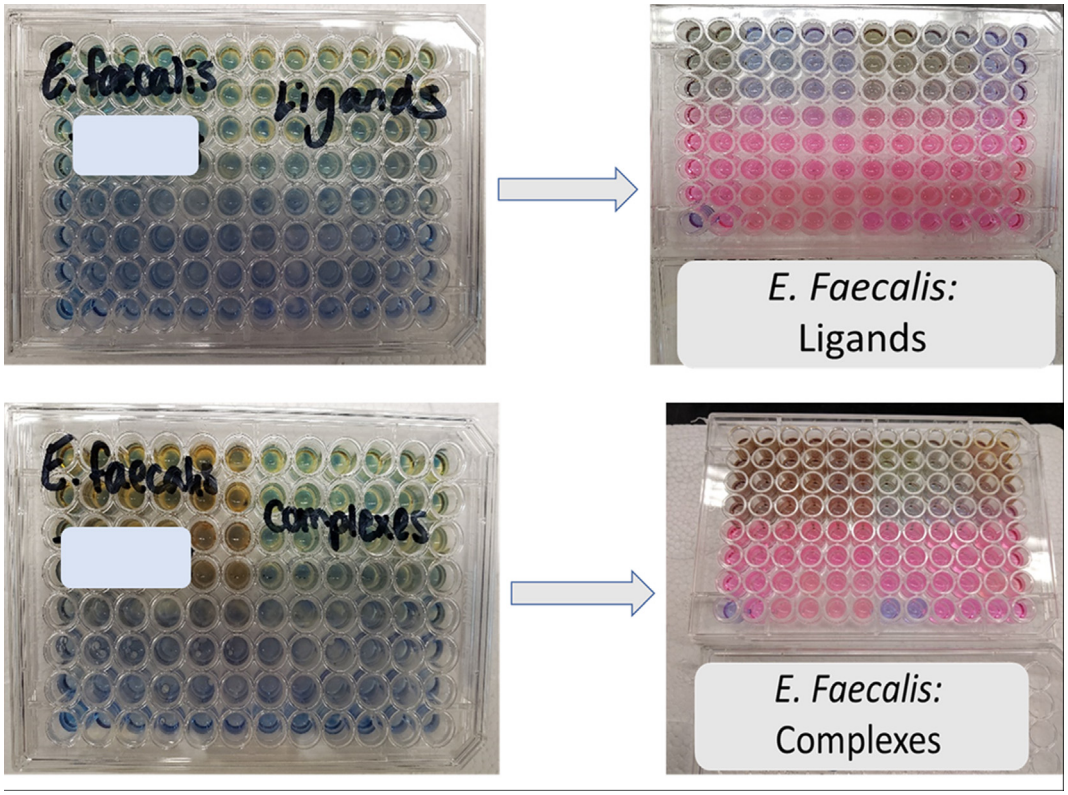

Fig. 7. Antimicrobial profile of the complexes from the resazurin micro-dilution assay.

Table 2
Antimicrobial profile of the complexes against bacteria.

Compound	Estimated MIC (μM) Bacterium *E. faecalis*	*S. pyogenes*	*P. aeruginosa*	*K. pneumoniae*
L1	50	***	6.25	25
L2	50		6.25	25
L3	50		6.25	25
L4	50		6.25	25
L5	50		6.25	25
L6	50		6.25	25
C1	25		25	12.5
C2	25		25	12.5
C3	25		25	12.5
C4	25		25	12.5
C5	25		25	12.5
C6	25		25	12.5

***See the main text.

compounds proved effective in reducing cell viability in HEK293T cell cultures, with 80% to 90% reduced cell viability at the highest concentrations tested (50 μM). Most compounds exhibited maximum effect at 24–48 h after addition of the compound. However, compound **C2** displayed a time-dependence, with cytotoxicity increasing as a function of time and achieving maximum cytotoxicity at 80 h post addition.

We next estimated lethal dose 50 (LD_{50}) values for each compound (Fig. 9). We identified two distinct groups of LD_{50} values for the six compounds tested. Compounds **C1** and **C3** displayed strongest cytotoxic effects with LD_{50} values $\geq$10 μM. The remaining compounds displayed slightly weaker cytotoxicity in the range of 20 μM to 40 μM. It can therefore be suggested that the thiosemicarbazone unit from ferrocene carboxaldehyde induces more biologically activity, and more generally, that cytotoxicity appears tunable. These results, coupled with the antimicrobial assays, demonstrate that these compounds to act as broad-range antibiotics.

4. Conclusion

The research results presented here describe the synthesis and reactivity of a novel series of CORMs. These complexes bearing thiosemicarbazone ligands slowly releases carbon monoxide when irradiated with ultraviolet light. We have also determined that the complexes are efficient at inhibiting the growth of both gram-negative and gram-positive bacteria. In addition, the complexes show good activity against gram-negative bacteria which is exciting given that agents that target these types of bacteria are difficult to find. Our results also demonstrate that our current generation CORMs display moderate antibiotic properties against both prokaryotic and eukaryotic cells. All six of the complexes displayed intrinsic cytotoxicity, as indicated by the relatively efficient cell killing.

Taken together, these results suggest that while the complexes release CO only slowly and likely to a small extent, good toxicity profiles were observed for the CORMs against bacteria and human cells, suggesting a broad mechanism of action. The physiochemical characteristics of the compounds is affected by the nature of the thiosemicarbazone kernel. So, speculating further, the CORM compounds represent a potential vehicle for future development of targeted antibiotic and antitumor compounds.

Credit authorship contribution statement

Madelyn L. Lawrence: Investigation, Writing - original draft. **Steven M. Shell:** Methodology, Investigation, Writing - review & editing. **Floyd A. Beckford:** Conceptualization, Methodology, Writing - review & editing, Investigation.

Declaration of Competing Interest

The authors declare that they have no known competing financial interests or personal relationships that could have appeared to influence the work reported in this paper.

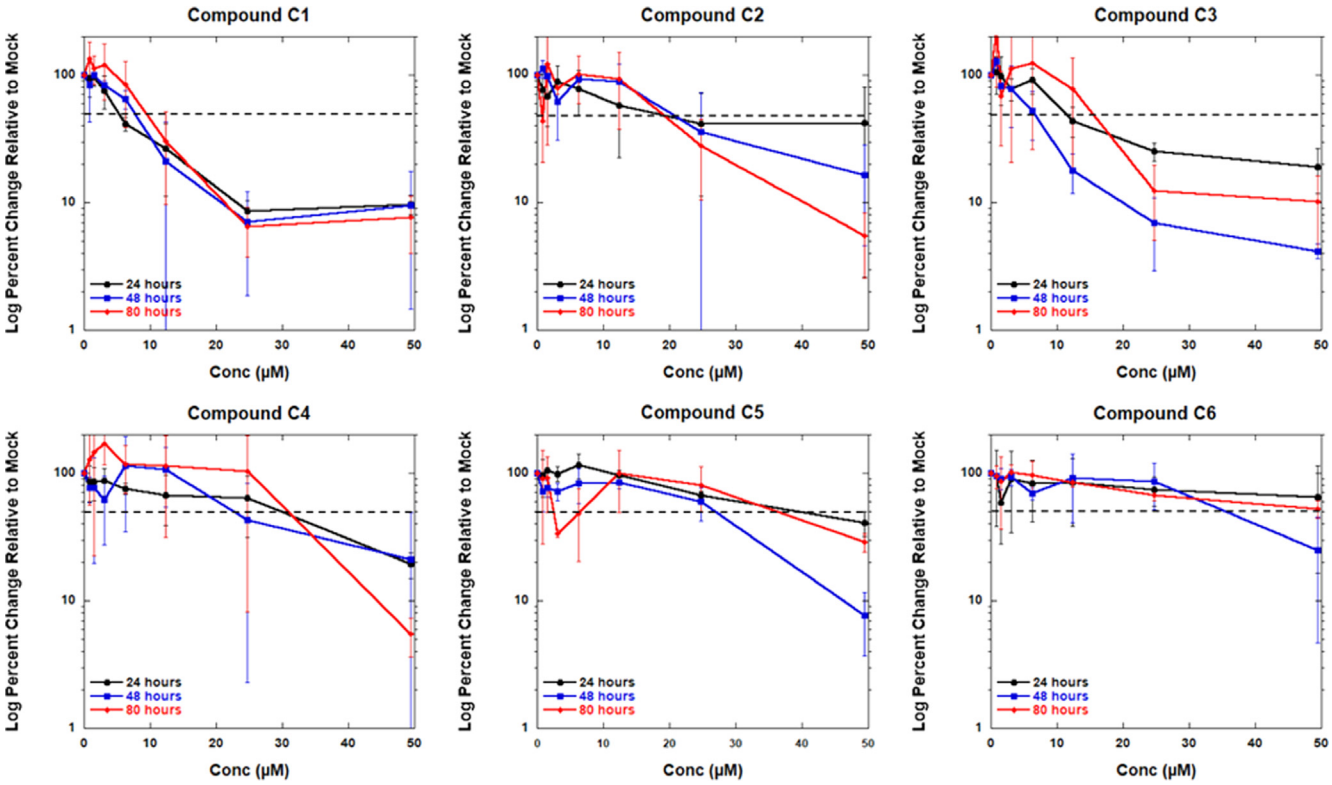

Fig. 8. Cytotoxicity profiles of the complexes against HEK293T human cells. HEK293T cells were cultured in medium supplemented with DMSO solvent or increasing concentration of compounds **C1**-**C6**. MTT metabolism assay was performed at 24, 48, and 80 h post addition of the compounds. Dashed line indicates loss of 50% cell viability in the culture. Error bars represent the standard deviation of three independent experiments.

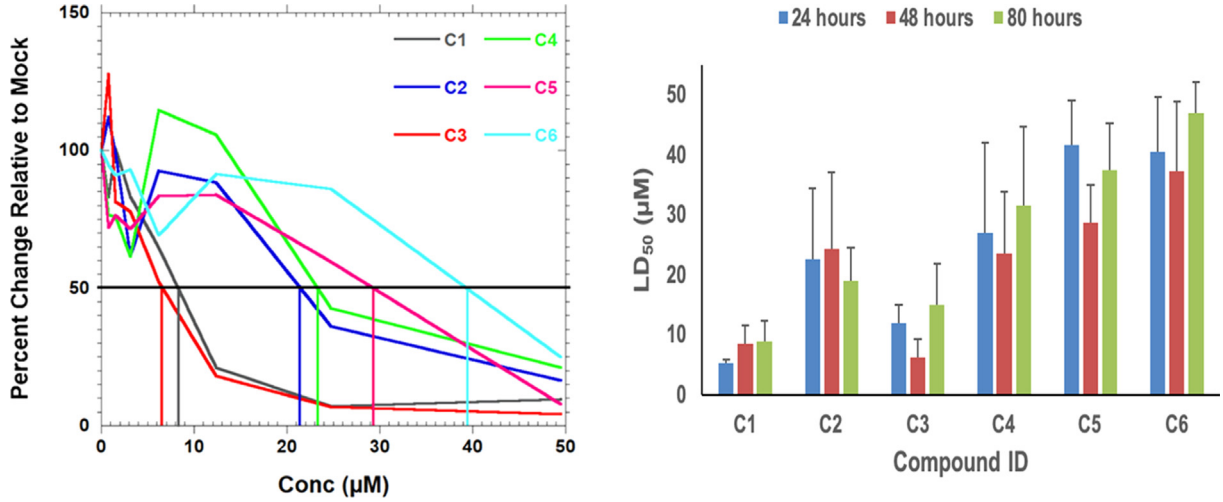

Fig. 9. Estimated graphical estimation of LD_{50} values in HEK293T human cell line. LD_{50} values were estimated graphically for data sets at 24, 48, and 80 h post addition of compound. Error bars represent the mean of three independent experiments.

Acknowledgements

MLL would like to thank the Department of Natural Sciences at the University of Virginia's College at Wise for Fellowships in the Natural Sciences to carry out this work. FAB is supported through the Van Daniel III Endowed Chair in Chemistry. The authors would also like to thank Dr. Robin Woodard for her assistance with the antimicrobial assays.

Appendix A. Supplementary data

Supplementary data to this article can be found online at https://doi.org/10.1016/j.ica.2020.119548.

References

[1] J.S. Ward, Organomet. Chem. (2016) 140–176.
[2] G. Kikuchi, T. Yoshida, M. Noguchi, Biochem. Biophys. Res. Commun. 338 (2005) 558–567.
[3] S.W. Ryter, L.E. Otterbein, D. Morse, A.M.K. Choi, Heme Oxyg. Biol. Med. (2002) 19–29.
[4] R. Motterlini, L.E. Otterbein, Nat. Rev. Drug Discov. 9 (2010) 728–743.
[5] S.W. Ryter, A.M.K. Choi, Korean J. Intern. Med. 28 (2013) 123–140.
[6] U. Schatzschneider, Br. J. Pharmacol. 172 (2015) 1638–1650.
[7] S. García-Gallego, G.J.L. Bernardes, Angew. Chemie - Int. Ed. 53 (2014) 9712–9721.
[8] B.E. Mann, R. Motterlini, Chem. Commun. (2007) 4197–4208.

[9] R. Alberto, R. Motterlini, Dalt. Trans. (2007) 1651–1660.
[10] C.S. Allardyce, P.J. Dyson, Platin. Met. Rev. 45 (2001) 62–69.
[11] D. Salvemini, Z.Q. Wang, J.L. Zweier, A. Samouilov, H. Macarthur, T.P. Misko, M.G. Currie, S. Cuzzocrea, J.A. Sikorski, D.P. Riley, Science 286 (1999) 304–306.
[12] K. Aston, N. Rath, A. Naik, U. Slomczynska, O.F. Schall, D.P. Riley, Inorg. Chem. 40 (2001) 1779–1789.
[13] H. Meyer, F. Winkler, P. Kunz, A.M. Schmidt, A. Hamacher, M.U. Kassack, C. Janiak, Inorg. Chem. 54 (2015) 11236–11246.
[14] H. Meyer, M. Brenner, S.P. Höfert, T.O. Knedel, P.C. Kunz, A.M. Schmidt, A. Hamacher, M.U. Kassack, C. Janiak, Dalt. Trans. 45 (2016) 7605–7615.
[15] I.J.S. Fairlamb, A.K. Duhme-Klair, J.M. Lynam, B.E. Moulton, C.T. O'Brien, P. Sawle, J. Hammad, R. Motterlini, Bioorganic Med. Chem. Lett. 16 (2006) 995–998.
[16] D.X. West, A.E. Liberta, S.B. Padhye, R.C. Chikate, P.B. Sonawane, A.S. Kumbhar, R.G. Yerande, Coord. Chem. Rev. 123 (1993) 49–71.
[17] A.G. Quiroga, J.M. Pérez, I. López-Solera, J.R. Masaguer, A. Luque, P. Román, A. Edwards, C. Alonso, C. Navarro-Ranninger, J. Med. Chem. 41 (1998) 1399–1408.
[18] J.P. Scovill, D.L. Klayman, C. Lambros, G.E. Childs, J.D. Notsch, J. Med. Chem. 27 (1984) 87–91.
[19] D.X. West, C.S. Carlson, K.J. Bouck, A.E. Liberta, Transit. Met. Chem. 16 (1991) 271–275.
[20] A.M. Thomas, A.D. Naik, M. Nethaji, A.R. Chakravarty, Inorganica Chim. Acta 357 (2004) 2315–2323.
[21] S.K. Chattopadhyay, S. Ghosh, Inorganica Chim. Acta 131 (1987) 15–20.
[22] D.R. van Staveren, N. Metzler-Nolte, Chem. Rev. 104 (2004) 5931–5985.
[23] M.F.R. Fouda, M.M. Abd-Elzaher, R.A. Abdelsamaia, A.A. Labib, Appl. Organomet. Chem. 21 (2007) 613–625.
[24] P. Meunier, I. Ouattara, B. Gautheron, J. Tirouflet, D. Camboli, J. Besançon, Eur. J. Med. Chem. 26 (1991) 351–362.
[25] P. Köpf-Maier, H. Köpf, E.W. Neuse, Angew. Chemie Int. Ed. English 23 (1984) 456–457.
[26] C. Biot, N. François, L. Maciejewski, J. Brocard, D. Poulain, Bioorg. Med. Chem. Lett. 10 (2000) 839–841.
[27] T. Itoh, S. Shirakami, N. Ishida, Y. Yamashita, T. Yoshida, H.-S. Kim, Y. Wataya, Bioorg. Med. Chem. Lett. 10 (2000) 1657–1659.
[28] C.L. Ferreira, C.B. Ewart, C.A. Barta, S. Little, V. Yardley, C. Martins, E. Polishchuk, P.J. Smith, J.R. Moss, M. Merkel, M.J. Adam, C. Orvig, Inorg. Chem. 45 (2006) 8414–8422.
[29] O. Payen, S. Top, A. Vessières, E. Brulé, M.-A. Plamont, M.J. McGlinchey, H. Müller-Bunz, G. Jaouen, J. Med. Chem. 51 (2008) 1791–1799.
[30] A. Goel, D. Savage, S.R. Alley, P.N. Kelly, D. O'Sullivan, H. Mueller-Bunz, P.T.M. Kenny, J. Organomet. Chem. 692 (2007) 1292–1299.
[31] A. Vessières, S. Top, W. Beck, E. Hillard, G. Jaouen, Dalt. Trans. (2006) 529–541.
[32] J.S. Casas, M.V. Castao, M.C. Cifuentes, A. Sánchez, J. Sordo, Polyhedron 21 (2002) 1651–1660.
[33] J.E.J.C. Graúdo, N.L. Speziali, A. Abras, M. Hörner, C.A.L. Filgueiras, Polyhedron 18 (1999) 2483–2489.
[34] H.G. Daniels, O.G. Fast, S.M. Shell, F.A. Beckford, J. Photochem. Photobiol. A Chem. 374 (2019) 84–94.
[35] B.J. Aucott, J.S. Ward, S.G. Andrew, J. Milani, A.C. Whitwood, J.M. Lynam, A. Parkin, I.J.S. Fairlamb, Inorg. Chem. 56 (2017) 5431–5440.
[36] R. Mede, S. Gläser, B. Suchland, B. Schowtka, M. Mandel, H. Görls, S. Krieck, A. Schiller, M. Westerhausen, Inorganics 5 (2017) 8.
[37] N.J. Farrer, L. Salassa, P.J. Sadler, Dalt. Trans. (2009) 10690–10701.
[38] N.J. Farrer, P.J. Sadler, Aust. J. Chem. 19 (2008) 669–674.
[39] K. Szaciłowski, W. Macyk, A. Drzewiecka-Matuszek, M. Brindell, G. Stochel, Chem. Rev. 105 (2005) 2647–2694.
[40] M. Wrighton, Chem. Rev. 74 (1974) 401–430.
[41] N. Palavutitotai, A. Jitmuang, S. Tongsai, P. Kiratisin, N. Angkasekwinai, PLoS One 13 (2018) e0193431.
[42] M. Bassetti, E. Righi, A. Carnelutti, E. Graziano, A. Russo, Expert Rev. Anti. Infect. Ther. 16 (2018) 749–761.
[43] C.M. Marr, T.A. Russo, Expert Rev. Anti. Infect. Ther. 17 (2019) 71–73.